Metabolism Clinical and Experimental 121 (2021) 154803

Contents lists available at ScienceDirect

Metabolism Clinical and Experimental

journal homepage: www.metabolismjournal.com

Lipids activate skeletal muscle mitochondrial fission and quality control networks to induce insulin resistance in humans

Christopher L. Axelrod [a,b,c], Ciaran E. Fealy [c], Melissa L. Erickson [a,c], Gangarao Davuluri [a,d], Hisashi Fujioka [e,f], Wagner S. Dantas [a], Emily Huang [c], Kathryn Pergola [a,b], Jacob T. Mey [a,c], William T. King [a,b], Anny Mulya [c], Daniel Hsia [g], Bartolome Burguera [h], Bernard Tandler [f,i], Charles L. Hoppel [a,f,j], John P. Kirwan [a,c,*]

[a] Integrated Physiology and Molecular Medicine Laboratory, Pennington Biomedical Research Center, Baton Rouge, LA 70808, USA
[b] Department of Translational Services, Pennington Biomedical Research Center, Baton Rouge, LA 70808, USA
[c] Department of Inflammation and Immunity, Lerner Research Institute, Cleveland Clinic, Cleveland, OH 44195, USA
[d] Sarcopenia and Malnutrition Laboratory, Pennington Biomedical Research Center, Baton Rouge, LA 70808, USA
[e] Cryo-Electron Microscopy Core, Case Western Reserve University, Cleveland, OH 44109, USA
[f] Center for Mitochondrial Diseases, Case Western Reserve University School of Medicine, Cleveland, OH 44106, USA
[g] Clinical Trials Unit, Pennington Biomedical Research Center, Baton Rouge, LA 70808, USA
[h] Endocrinology and Metabolism Institute, Cleveland Clinic, Cleveland, OH, 44195, USA
[i] Department of Biological Sciences, Case Western Reserve University School of Dental Medicine, Cleveland, OH 44106, USA
[j] Department of Pharmacology, Case Western Reserve University, Cleveland, OH 44109, USA

ARTICLE INFO

Article history:
Received 16 March 2021
Accepted 31 May 2021
Available online xxxx

ABSTRACT

Background and aims: A diminution in skeletal muscle mitochondrial function due to ectopic lipid accumulation and excess nutrient intake is thought to contribute to insulin resistance and the development of type 2 diabetes. However, the functional integrity of mitochondria in insulin-resistant skeletal muscle remains highly controversial.
Methods: 19 healthy adults (age:28.4 ± 1.7 years; BMI:22.7 ± 0.3 kg/m^2) received an overnight intravenous infusion of lipid (20% Intralipid) or saline followed by a hyperinsulinemic-euglycemic clamp to assess insulin sensitivity using a randomized crossover design. Skeletal muscle biopsies were obtained after the overnight lipid infusion to evaluate activation of mitochondrial dynamics proteins, ex-vivo mitochondrial membrane potential, ex-vivo oxidative phosphorylation and electron transfer capacity, and mitochondrial ultrastructure.
Results: Overnight lipid infusion increased dynamin related protein 1 (DRP1) phosphorylation at serine 616 and PTEN-induced kinase 1 (PINK1) expression ($P = 0.003$ and $P = 0.008$, respectively) in skeletal muscle while reducing mitochondrial membrane potential ($P = 0.042$). The lipid infusion also increased mitochondrial-associated lipid droplet formation ($P = 0.011$), the number of dilated cristae, and the presence of autophagic vesicles without altering mitochondrial number or respiratory capacity. Additionally, lipid infusion suppressed peripheral glucose disposal ($P = 0.004$) and hepatic insulin sensitivity ($P = 0.014$).
Conclusions: These findings indicate that activation of mitochondrial fission and quality control occur early in the onset of insulin resistance in human skeletal muscle. Targeting mitochondrial dynamics and quality control represents a promising new pharmacological approach for treating insulin resistance and type 2 diabetes.
Clinical trial registration: NCT02697201, ClinicalTrials.gov

1. Introduction

Insulin resistance is a key pathophysiological mechanism in the development and progression of type 2 diabetes. Abnormalities in lipid metabolism and ectopic lipid accumulation are known to directly contribute to the onset of insulin resistance [1]. However, there are major gaps in our understanding of how the pathways and organelles linking excess lipid intermediates, such as diacylglycerol and ceramides, contribute to or cause impairments in insulin action [2,3]. Since mitochondria are central in controlling nutrient oxidation and release of cellular energy, they may also lie at the nexus of a myriad of metabolic diseases [4]. Patients with obesity or type 2 diabetes exhibit a number of mitochondrial abnormalities, including reduced number, increased swelling, and augmented cristae [5]. These observations support the hypothesis that mitochondrial dysfunction may regulate lipid-induced insulin resistance. However, there are contrary observations describing intact or even elevated skeletal muscle oxidative function in both humans and

* Corresponding author at: Integrated Physiology and Molecular Medicine Laboratory, Pennington Biomedical Research Center, 6400 Perkins Road, Baton Rouge, LA 70808, Location: L-4030, USA.
E-mail address: john.kirwan@pbrc.edu (J.P. Kirwan).

https://doi.org/10.1016/j.metabol.2021.154803
0026-0495/

rodents with type 2 diabetes [6,7]. In addition to oxidative functions, mitochondrial morphology and ultrastructure are highly sensitive to the bioenergetic status of the cell. These observations led to alternative hypotheses that mitochondrial membrane dynamics may mediate insulin resistance by regulating excess nutrient availability [8,9].

Mitochondrial dynamics is a highly conserved process whereby routine cycles of fission and fusion on the outer and inner mitochondrial membranes maintain network quality and integrity [10–12]. Mitochondrial fission is regulated by recruitment of cytosolic dynamin related protein 1 (DRP1) to the outer mitochondrial membrane (OMM) in coordination with mitochondrial fission protein-1 (Fis1) and/or mitochondrial fission factor (Mff) [13,14]. DRP1 is recruited to the OMM, in part, by phosphorylation of the serine 616 residue ($DRP1^{Ser616}$), which promotes fission activity [15]. DRP1 forms multimeric spirals around the outer membrane and initiates a fission event by membrane constriction [16]. Critically, DRP1-mediated mitochondrial fission results in depolarization of membrane potential ($\Delta\Psi_m$) in excised mitochondrial network fragments. Excised mitochondria may then recover membrane potential and, where fusion activity is high, rejoin the network [17]. Alternatively, network fragments can be tagged for autophagy by PTEN-induced putative kinase-1 (PINK1) which rapidly accumulates on depolarized mitochondrial membranes [18]. Mitochondrial fusion occurs in two discrete yet highly coordinated steps on the OMM and inner mitochondrial membrane (IMM). First, adjacent mitochondria become tethered by homotypic or heterotypic interactions between mitofusin 1 and 2 (MFN1 and MFN2, respectively) [19]. Optic Atrophy-1 (OPA1) then initiates tethering of the IMM to complete integration of adjacent mitochondrion [20].

Induction of DRP1-mediated mitochondrial fission by long chain fatty acids has been previously observed in murine and in vitro models of insulin resistance [21]. Additionally, we and others have demonstrated that exercise training and weight loss can improve mitochondrial dynamics primarily by reducing $DRP1^{Ser616}$ activity in patients with obesity and prediabetes [8,22]. However, studying the dynamics, structure, and function of mitochondria in human insulin-resistant skeletal muscle is confounded by long term metabolic adaptations to both obesity and type 2 diabetes. To overcome this problem, we performed intravenous lipid infusions in sedentary but otherwise healthy humans to induce insulin resistance and assess changes in mitochondrial dynamics, structure, and function using a randomized crossover study design. We hypothesized that lipid infusion would increase DRP1-mediated mitochondrial fission in skeletal muscle independent of function and content, consequently reducing peripheral insulin sensitivity. We show that accumulation of lipid within and surrounding skeletal muscle mitochondria triggers fission, fragmentation and mitophagy by DRP1 activation, dampening of $\Delta\Psi_m$ and accumulation of PINK1 on depolarized mitochondrial membranes. In contrast, mitochondrial respiratory function and mitochondrial content and ultrastructure were unperturbed despite the onset of insulin resistance. These data suggest that mitochondrial quality control may be a key initiator of skeletal muscle insulin resistance in humans.

2. Research design and methods

2.1. Participants

19 sedentary but otherwise healthy individuals with a BMI <25 kg/m^2 completed the study. Participants were weight stable (>5 kg weight change) in the 6 months before enrollment, exercised for less than 30 min of moderate/high intensity exercise two or more times weekly, were non-smokers for >5 years, did not have an immediately family history of type 2 diabetes, and were free of prescription medications and significant metabolic, cardiac, cerebrovascular, hematological, pulmonary, gastrointestinal, liver, renal, or endocrine disease or cancer that would affect the outcome measures or subject safety. Female participants were not pregnant or nursing, experienced normal menstrual function, were not using hormonal contraceptives, and were evaluated during the mid-follicular phase of the menstrual cycle. All participants received a history and physical examination at the time of screening to rule out contraindications to study procedures. All participants provided written informed consent and research procedures were approved by the Cleveland Clinic and Pennington Biomedical Research Center Institutional Review Board. The Dynamics of Muscle Mitochondria (DYNAMMO) trial was registered on clinicaltrials.gov (NCT02697201) prior to enrollment of study participants.

2.2. Experimental design

Eligible participants were prospectively randomized (1:1) in blocks of 4 by a blinded statistician to receive a constant-rate low dose infusion (0.55 mL/kg/h) of normal saline or a 20% lipid emulsion (Intralipid® 20%; Baxter International Inc.; Deerfield, IL) for 12 h overnight (12 ± 0.2 h) in a crossover design. Before the infusion, participants completed a 2-day metabolic control period consisting of 2 overnight stays on the inpatient unit as described previously [22]. During the inpatient control periods, participants were provided with a weight maintenance isocaloric diet (total kcal/day = resting metabolic rate × 1.25; 55% carbohydrate, 35% fat, and 10% protein) derived from indirect calorimetry measures conducted at the beginning of the inpatient control period. Participants returned to the inpatient unit for the second study arm approximately 2–4 weeks later. The primary outcome of the study was change in skeletal muscle $DRP1^{Ser616}$ phosphorylation from saline to lipid infusion. Secondary outcomes included the effects of lipid infusion on proteins that regulate mitochondrial dynamics, mitochondrial membrane potential and fragmentation, mitochondrial function and ultrastructure, and insulin sensitivity.

2.3. Body composition

At ~06:00 following the first overnight stay, body composition and anthropometrics were measured as described previously [22]. Briefly, height and weight were measured in a hospital gown using standard techniques. Dual-energy X-ray absorptiometry (Lunar iDXA; Madison, WI) was then used to determine whole body fat and lean mass. Estimation of fat and lean tissue content was obtained from iDXA software according to the manufacturer's instructions.

2.4. Aerobic capacity

At ~19:00 on the evening of the first overnight stay, maximal oxygen consumption was determined using an incremental, graded treadmill exercise test as described previously [22]. Criteria for determination of a maximal test were as follows: 1) oxygen consumption plateau (<150 mL/ min), 2) heart rate within 15 beats of age-predicted max, 3) respiratory exchange ratio > 1.15, and/or 4) volitional fatigue. Participants were required to achieve 3 of 4 criteria in order for the test to be considered maximal.

2.5. Insulin sensitivity

Insulin sensitivity was determined on the 3rd inpatient day using a five hour, euglycemic-hyperinsulinemic clamp (90 mg/dL, 40 mU·m^{-2}·min^{-1}), as described previously [22]. Briefly, a primed (3.28 mg/kg) continuous (0.036 mg·kg^{-1} ·min^{-1}) infusion of D-[6,6-$^2H_2$]glucose began at −120 min and continued throughout the procedure to calculate hepatic glucose production (HGP). At 0 min, simultaneous infusion of insulin (constant) and 20% dextrose (variable) began. Arterialized heated-hand venous blood was sampled at 5 min intervals (YSI 2900 Biochemistry Analyzer; YSI, Inc., Yellow Springs, OH), and the glucose infusion rate (GIR) was adjusted in order to maintain plasma glucose at 90 mg/dL according to the correction algorithm of DeFronzo et al. [23]. Insulin sensitivity was then calculated as insulin-

stimulated glucose metabolism (M; $mg \cdot kg^{-1} \cdot min^{-1}$) divided by plasma insulin (I; μU/mL) over a 30-min steady state period. Plasma for assessing glucose kinetics was deproteinized, extracted and derivatized before analysis by gas chromatography–mass spectrometry as previously described [24]. Isotopic enrichment (mole percent excess) was determined by fitting the fractional abundances (M + 2; *m/z* 330)/(M0; m/z 328) against a calibration curve. The rate of glucose appearance was then derived using the Steele Eq. [25]. Whole body respiratory exchange ratios (RER) and substrate metabolism were determined basally and under insulin-stimulated conditions via indirect calorimetry as previously described (Vmax Encore; Viasys, Yorba Linda, CA) [26]. Metabolic flexibility was calculated as the change in rate of fat oxidation from basal to insulin-stimulated conditions.

2.6. Muscle tissue procurement

Skeletal muscle specimens were obtained from the medial *vastus lateralis* using a modified Bergström biopsy technique at 08:00 (± 30 min) [27]. Upon collection, samples were dissected of fat and connective tissue, and immediately placed into preservation media or frozen in liquid nitrogen for protein studies. All muscle samples were then stored at −140 °C until the time of analysis.

2.7. Tissue preparation and Western blot analysis

Muscle homogenates were prepared as described previously [22]. Briefly, muscle tissue was homogenized using a Polytron immersion disperser in ice-cold Cell Extraction Buffer (Invitrogen) with added protease inhibitor cocktail, 5 mM phenylmethylsulfonyl fluoride (Sigma), 1 mM sodium orthovanadate (Sigma) and Phos-STOP (Roche Applied Sciences, Indianapolis, IN). Homogenates were then centrifuged for 10 min at 14,000 x *g*, the supernatant decanted, and tissue lysates stored at −80 °C until the time of analysis. Protein concentrations were measured using a BCA protein assay kit (Pierce Biotechnology, Rockford, IL). 30 μg (0.75 μg/μL) of muscle lysate were solubilized in Laemmli sample buffer containing 5% β-mercaptoethanol and boiled for 5 min. 40 μL sample was then loaded onto 4–20% Tris Glycine gels (Novex) and separated via sodium dodecyl sulfate polyacrylamide gel electrophoresis at 125 V for 1.5 h (Invitrogen). The gels were transferred to polyvinylidene fluoride membranes (Bio-Rad), and blocked with 5% bovine serum albumin (BSA) in Tris-buffered saline with 0.1% Tween-20 (TBST) for 1 h. Membranes were then incubated overnight with anti-$DRP1^{Ser616}$ (Cell Signaling Technology; catalog no. 3455), anti-DRP1 (Cell Signaling Technology; catalog no. 8570), anti-MFF^{Ser146} (Cell Signaling Technology; catalog no. 49281), anti-MFF (Cell Signaling Technology; catalog no. 84580), anti-Mid49 ProteinTech; catalog no. 20164–1-AP), anti-Mid51 (ProteinTech; catalog no. 16413–1-AP), anti-PINK1 (Abcam ab23707), anti-MFN1 (R & D Systems; Minneapolis, MN, catalog no. AF7880), anti-MFN2 (Cell Signaling Technology; catalog no. 9482), and anti-OPA1 (Abnova; catalog no. 12083), anti-FIS1 (Thermo Fisher Scientific; catalog no. PA1–41082), anti-Parkin (Cell Signaling Technology; catalog no. 4211), and anti-Vinculin (Cell Signaling Technology; catalog no. 18799) antibodies. Membranes were washed with TBST and incubated with species-specific horseradish peroxidase-conjugated secondary antibodies (GE Healthcare; catalog no. NA931). Immunoreactive proteins were visualized by enhanced chemiluminescence reagent (ECL Prime; GE Healthcare) and quantified by densitometric analysis using ImageJ 4 [28]. Visible bands reactive against an internal control were subject to quantification. Values were expressed as fold induction relative to saline normalized to loading control (Vinculin).

2.8. Oxidative phosphorylation (OXPHOS) and electron transfer (ET) capacity of permeabilized muscle fibers

OXPHOS and ET capacity were determined ex-vivo from permeabilized muscle fibers as described previously [29]. At the time of biopsy, 10–15 mg of muscle tissue was immediately placed into BIOPS (50 mM K + -MES, 20 mM taurine, 0.5 mM dithiothreitol, 6.56 mM $MgCl_2$, 5.77 mM ATP, 15 mM phosphocreatine, 20 mM imidazole, pH 7.1, adjusted with 5 N KOH at 0 °C, 10 mM Ca–EGTA buffer, 2.77 mM CaK_2EGTA + 7.23 mM K_2EGTA; 0.1 mM free calcium) solution. The muscle bundles were then mechanically separated under a dissection microscope, placed into fresh BIOPS containing saponin (50 μg/mL), and gently agitated at 4 °C for 20 min. The fibers were then transferred to a mitochondrial respiration medium (110 mM sucrose, 60 mM K + -lactobionate, 0.5 mM EGTA, 3 mM $MgCl_2$, 20 mM taurine, 10 mM KH2PO4, 20 mM HEPES adjusted to pH 7.1 with KOH at 37 °C; and 1 g/L de-fatted BSA), blotted on filter paper, and weighed. 2–5 mg of permeabilized fiber bundles were transferred into the Oxygraph chamber containing 2 mL of MiR05, the oxygen content of the chamber was raised to ~450 μM, and the background respiration was allowed to stabilize. OXPHOS and ET capacity was determined using the following concentrations of substrates, uncouplers, and inhibitors: malate (2 mM), pyruvate (2.5 mM), ADP (2.5 mM), glutamate (10 mM), succinate (10 mM), palmitoylcarnitine (10 μM), duroquinol (0.5 mM), tetramethyl-*p*-phenylenediamine (TMPD, 0.5 μM), ascorbate (2 mM), carbonylcyanide-*p*-trifluoromethoxyphenylhydrazone (FCCP, 0.5 μM increment), rotenone (75 nM), antimycin A (125 nM) and sodium azide (200 mM). Oxygen flux was normalized to tissue wet weight (mg). Cytochrome c (10 μM) was added to confirm mitochondrial outer membrane integrity.

2.9. Mitochondrial membrane potential and network fragmentation

Mitochondrial membrane potential and morphology was assessed from thin tissue sections using the fluorophores TMRM (Invitrogen) and MitoTracker Deep Red (Invitrogen) as previously described [30] with the following modifications. Immediately upon collection, 5 mg of tissue was placed into a BIOPS solution and warmed in a 37 °C water-jacketed incubator containing 5% CO_2. The tissue section was then incubated in a mixture containing 200 nM TMRM, 150 nM MitoTracker Deep Red, and 10 μg/mL DAPI for 30 min. After staining, the tissue section was rinsed three times with PBS, centered on a glass petri dish, and placed on a temperature and humidity-controlled stage. Images were obtained at 63× and 150× magnification in 5-μm sections using an inverted confocal microscope (SP8; Leica Microsystems) by an independent research technician who was blinded to the experimental trial. 10 nM FCCP was added at the end of image acquisition as a negative control. 10–15 images capturing both TMRM and MitoTracker Deep Red florescent intensity were obtained per participant, averaged, and then quantified as the percent change from the saline to lipid condition. An index of mitochondrial fragmentation was also calculated from merged z-stacks [31] using segmented particle analysis in ImageJ 4 [28].

2.10. Mitochondrial ultrastructure and content

Ultrastructural morphology of muscle tissue was examined using transmission electron microscopy as previously described [32]. Briefly, 15–20 mgs of muscle tissue were fixed by immersion in a triple aldehyde-DMSO mixture [33]. Tissue blocks were post-fixed in ferrocyanide-reduced osmium tetroxide, soaked in acidified uranyl acetate, dehydrated in ascending concentrations of ethanol, passed through propylene oxide, and embedded in Poly/Bed resin. Thin sections were stained with acidified uranyl acetate [34] followed by modified Sato's triple lead stain [35]. Mitochondrial content was determined by manual tracing of only clearly discernible outlines of mitochondria on transmission electron micrographs and quantified using threshold analysis in ImageJ 4 [28].

2.11. ATP content

ATP concentrations were determined in deproteinated tissue samples using a commercially available fluorometric assay (Abcam) per manufacturer instruction. Briefly, snap-frozen tissue (10 mg) was homogenized in 100 μL ice cold 2 N perchloric acid (PCA) using a bead-beating grinder and lysis system (FastPrep-24; MP Biomedicals) and then incubated on ice for 45 min. The resulting homogenate was then centrifuged at 13,000 ×*g* for 2 min at 4 °C. The supernatant was then transferred to a fresh tube and the volume was brought to 500 uL with the ATP assay buffer. Excess PCA was precipitated by adding 100 μL of ice-cold 2 M KOH, vortexing briefly, and maintaining a neutral pH. The samples were centrifuged at 13,000 ×*g* for 15 min at 4 °C and the supernatant was collected for ATP measurement. Standards and samples were plated in duplicate into a 96-well black walled plate, the ATP reaction mix was added, and the plate was incubated at room temperature for 30 min protected from light. The reactions were analyzed with a microplate reader (Ex/Em = 535/587 nm). Data are expressed as nmols of ATP per mg tissue wet weight.

2.12. Citrate synthase activity

Enzymatic activity of citrate synthase was determined in snap-frozen tissue (~10 mg) using a commercially available colorimetric assay (Sigma-Aldrich, St. Louis, MO, USA) as described previously [36]. Briefly, tissue was homogenized in 100 μL of ice cold 1× assay buffer and incubated on ice for 10 min. Homogenates were centrifuged at 10,000 ×*g* for 5 min at 4 °C to pellet tissue debris. The supernatant was transferred to a fresh tube, and protein content was assessed by BCA assay (Thermo Scientific). 10 μg of protein lysate suspended in 1× assay buffer containing 30 mM acetyl CoA and 10 mM DTNB was plated in duplicate on a 96-well plate. Absorbance was then measured on a plate reader set to kinetic mode (412 nm, 1.5 min duration, 10 s intervals) before and after the addition of 10 mM oxaloacetate. Data are expressed as nmols of activity per minute per mg protein.

2.13. mtDNA

mtDNA was determined as described previously [36]. Total DNA was extracted using commercially available reagents (DNeasy Blood and Tissue Kit; Qiagen). RT-qPCR was then performed using Power SYBR Green (Thermo Fisher Scientific) with primers directed against the mitochondrial encoded cytochrome *c* oxidase subunit II (*Cox2*) and the nuclear encoded *18S* [37]. Primer sequences can be found in Supplementary Table 1.

2.14. Biochemical analyses

Metabolic profiles, including cell counts and lipid concentrations, were analyzed on an automated platform as described previously [38]. Plasma free fatty acids were determined using a commercially available enzymatic assay (Abcam; ab65341). Insulin was determined by a commercially available competitive binding radioimmunoassay (Millipore; HI-14 K).

2.15. Power estimates

Participant sample size for the primary outcome variable (p-DRP1^{Ser616}) was calculated with the following input parameters: two tailed paired *t*-test (difference between two dependent means, α error probability = 0.05, Power (1-β error probability) = 0.95, and a standardized effect size (dz) = 1.08 (difference between p-DRP1^{Ser616} after saline and lipid infusion). A dz. was estimated using previous data from our laboratory in three individuals with obesity during lipid infusion since an estimate of variability was also available from this population. There was an increase in p-DRP1^{Ser616} from control to lipid

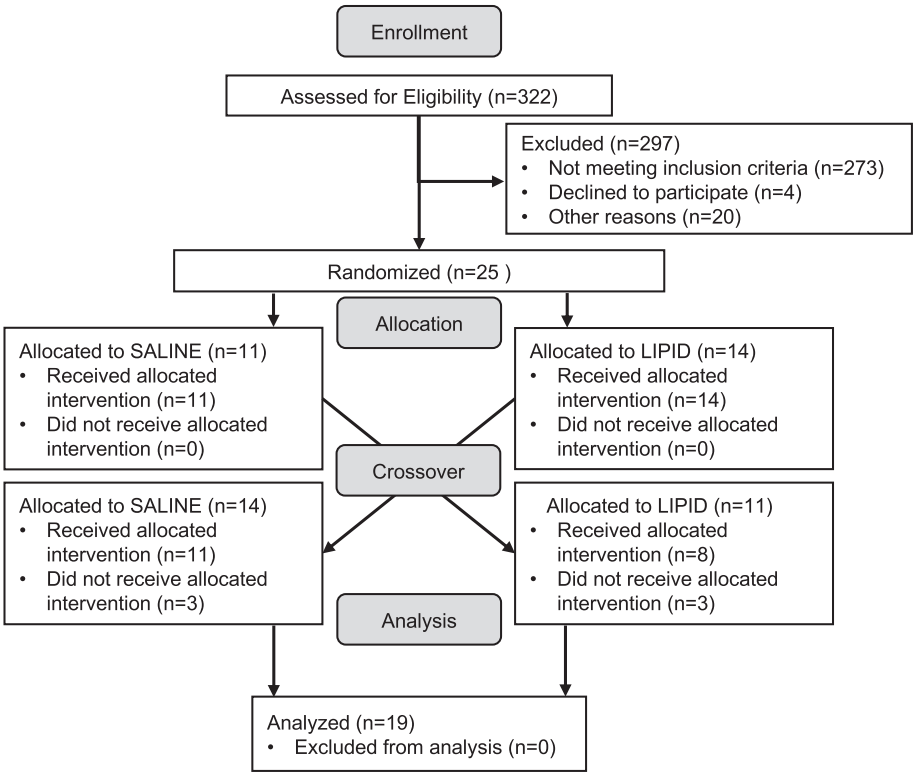

Fig. 1. CONSORT diagram depicting study enrollment, treatment allocation, and analysis.

infusion (0.30 ± 0.10 vs. 0.46 ± 0.17 AU). Subject sample size was estimated as $N = 14$ per group with a calculated actual power of 0.96 (critical $t = 2.16$) for within group effects. Therefore, allowing for potential dropout with the crossover design we expected that with a total sample size of $N = 19$–20 the study would be adequately powered to observe differences in p-DRP1^{Ser616} between conditions by a two tailed paired sample *t*-test.

2.16. Statistical analyses

Baseline differences between saline and lipid infusion were assessed by a paired sample *t*-test. Effects of treatment *x* time were assessed by two-way analysis of variance (ANOVA). Main effects were followed by Tukey's post-hoc test. Normality of distribution was assessed visually by a Q-Q plot and statistically by the Kolmogorov-Smirnov test. Homogeneity of variance was assessed by the Brown-Forsythe test. If sphericity was not met, the Greenhouse-Geisser correction was applied. All statistical analyses were performed using Prism 8 (GraphPad, San Diego, CA).

3. Results

3.1. Participants

A total of 322 individuals expressed interest in participation and were assessed for eligibility (Fig. 1), 25 were randomized, and 19 completed the saline and lipid-infusion arms of the protocol and were included in the final data analysis. The study population included 12 Caucasians, 4 Asians, 2 African Americans, and 1 Hispanic. There were no serious adverse events related to the study protocol. Baseline participant characteristics and effects of the lipid infusion on safety parameters and routine metabolic function are displayed in Tables 1 and 2, respectively. The lipid infusion modestly lowered circulating bilirubin (Δ = -0.3 mg/dL) and CO_2 (Δ = -0.8 mmol/L) while increasing mean platelet volume (MPV; Δ = 0.3 fL). The changes were within clinical range and all other safety parameters remained unchanged.

3.2. Skeletal muscle mitochondrial dynamics and structure

To determine the effects of elevated lipids on skeletal muscle mitochondrial dynamics, vastus lateralis biopsies were obtained after an overnight saline or lipid infusion and assessed for protein expression and activation (Fig. 2). We observed that p-DRP1^{Ser616} activation (1.0 ± 0.11 vs. 1.58 ± 0.28 fold, $P = 0.026$) and PINK1 expression (1.0 ± 0.19 vs. 1.77 ± 0.26 fold, $P = 0.008$) were increased by lipid infusion whereas proteins that regulate mitochondrial fusion were unaltered (Fig. 3A-F). To confirm that increased DRP1 and PINK1 expression were contributing to mitochondrial fragmentation, mitochondrial morphology was determined in skeletal muscle fibers ex-vivo by incubation in tetramethylrhodamine (TMRM) and Mitotracker Red. We observed that mitochondrial membrane potential ($\Delta\Psi_m$) was reduced following lipid infusion (100 ± 32.1 vs. 24.3 ± 13.1%, $P = 0.042$) (Fig. 4A-C). Further, morphometric analysis revealed increased mitochondrial fragmentation by lipids (100 ± 17.7 vs. 206.8 ± 19.1%, $P = 0.005$) (Fig. 4D). We then performed transmission electron microscopy to evaluate ultrastructural and morphological modifications to skeletal muscle mitochondria. Subsarcolemmal (SSM) and intermyofibrillar (IMF) mitochondria from the saline-infused tissue sections appeared normal in structure, abundance, and distribution (Fig. 4B). Lipid infusion resulted in modest dilation of SSM and IMF cristae, and the presence of autophagic vesicles in the perinuclear region. Mitochondrial content appeared similar (100 ± 12.0 vs. 113 ± 16.8%, $P = 0.56$) between conditions (Fig. 4E). The size of mitochondrial-associated lipid droplets was increased (100 ± 7.9 vs. 258 ± 47.0%, $P = 0.011$) by lipid infusion (Fig. 4F).

3.3. Skeletal muscle oxidative capacity

In order to distinguish changes in mitochondrial fission and fragmentation from respiratory function, OXPHOS and ET capacity were determined in permeabilized muscle fiber bundles (Fig. 5). We observed no differences in leak (L) or OXPHOS supported by pyruvate plus malate, glutamate, succinate in the presence of rotenone, and palmitoylcarnitine and octanoylcarnitine plus malate as substrates between saline and lipid infusion (Fig. 5A-B). The acceptor control ratio for ADP in the presence of pyruvate plus malate or palmitoylcarnitine plus malate was also unchanged by lipid infusion (Fig. 5C-D). Intracellular ATP (Fig. 5E), citrate synthase activity (Fig. 5F), and mtDNA content (Fig. 5G) were additionally unaltered by the lipid infusion.

Table 1
Participant characteristics.

	Mean	SEM
Sex (n)	(11 M; 8 F)	–
Age (years)	28	1.7
Height (cm)	170.4	2.1
BMI (kg/m^2)	22.7	0.3
Lean Mass (kg)	47.3	2.1
Fat (%)	31.3	2.2
Waist to Hip Ratio	0.8	0.0
HbA_{1c} (%)	5.2	0.1
VO_{2PEAK} (mL/kg/min)	37.8	2.4
Systolic Blood Pressure (mmHg)	110	2.8
Diastolic Blood Pressure (mmHg)	67	2.1

Table 2
Changes in circulating blood metabolites and immune function following saline and lipid infusion.

	Saline		Lipid		*P* value
	Mean	SEM	Mean	SEM	
Blood metabolites					
Total Protein (g/dL)	6.4	0.1	6.5	0.1	0.392
Albumin (g/dL)	3.8	0.1	3.9	0.1	0.429
Calcium (mg/dL)	8.7	0.1	8.8	0.1	0.360
Total Bilirubin (mg/dL)	0.7	0.1	0.4	0.1	<0.001
Alkaline Phosphatase (U/L)	48.1	2.6	47.2	2.3	0.499
AST (U/L)	17.8	1.1	18.8	1.8	0.495
BUN (mg/dL)	13.7	0.9	12.9	0.9	0.232
Creatinine (mg/dL)	0.7	0.0	0.7	0.0	0.607
Sodium (mmol/L)	137.8	0.5	137.7	0.6	0.821
Potassium (mmol/L)	3.9	0.0	3.9	0.1	0.451
Chloride (mmol/L)	104.4	0.6	104.1	0.5	0.692
CO2 (mmol/L)	22.7	0.3	21.9	0.4	0.021
Anion Gap (mmol/L)	12.7	0.6	13.9	0.7	0.058
ALT (U/L)	16.6	2.4	15.1	2.2	0.321
Immune function					
WBC (k/uL)	5.9	0.4	5.7	0.3	0.474
RBC (m/uL)	4.5	0.1	4.5	0.1	0.868
Hemoglobin (g/dL)	13.3	0.4	13.5	0.5	0.307
Hematocrit (%)	39.6	1.1	39.7	1.1	0.804
MCV (fL)	88.0	1.0	88.1	1.0	0.760
MCH (pG)	29.5	0.5	29.9	0.6	0.050
MCHC (g/dL)	33.5	0.3	33.9	0.4	0.116
RDW-CV (%)	12.4	0.2	12.4	0.2	0.648
Platelet Count (k/uL)	220.1	9.4	224.1	8.2	0.493
MPV (fL)	10.0	0.2	10.3	0.3	0.002
Blood lipids					
Triglyceride (mg/dL)	64.2	8.7	203.7	39.5	<0.001
Cholesterol (mg/dL)	153.2	6.9	158.7	8.5	0.162
HDL (mg/dL)	53.7	3.1	48.2	3.2	0.009
VLDL (mg/dL)	12.9	1.9	31.2	5.5	0.009
LDL (mg/dL)	86.6	6.3	72.9	6.1	0.004

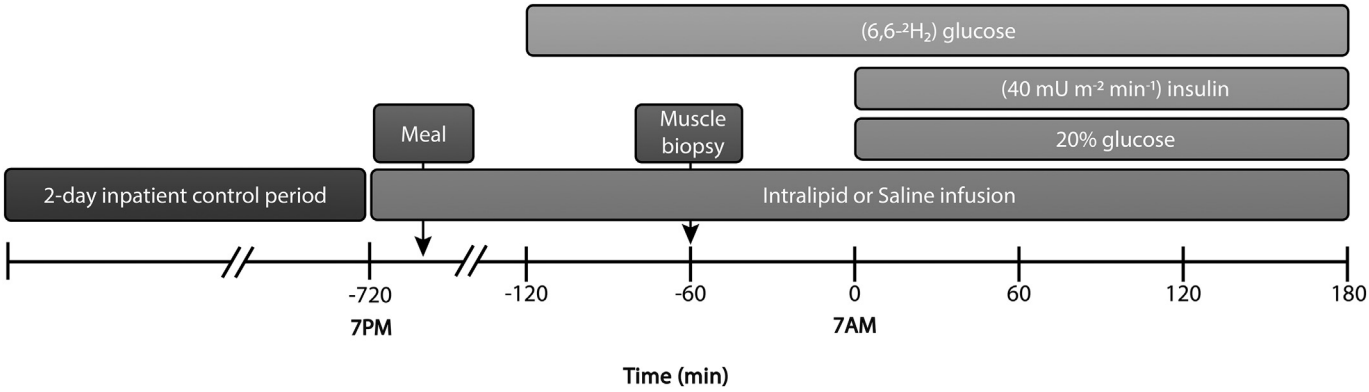

Fig. 2. Schematic illustration of the experimental design.

3.4. Insulin sensitivity and metabolic flexibility

Peripheral insulin sensitivity and action was determined by hyperinsulinemic-euglycemic clamp. Lipid infusion increased fasting plasma glucose (87.4 ± 1.2 vs. 91.9 ± 1.7 mg/dL, $P = 0.008$) and insulin (6.8 ± 0.7 vs. 8.9 ± 0.8 μU/mL, $P < 0.001$) concentrations (Fig. 6A-B). The insulin stimulated rate of glucose disposal (0.19 ± 0.02 vs. 0.13 ± 0.01 mg/kgFFM/min/μU/mL, $P = 0.004$) and suppression of hepatic glucose production (71.2 ± 12.2 vs. 29.6 ± 5.9%, $P = 0.014$) were both reduced by lipid infusion (Fig. 6C-E). As expected, FFA concentrations (0.58 ± 0.1 vs. 0.88 ± 0.1 mM, $P = 0.001$) were elevated by the lipid infusion (Fig. 7A). This was observed in concert with elevated circulating

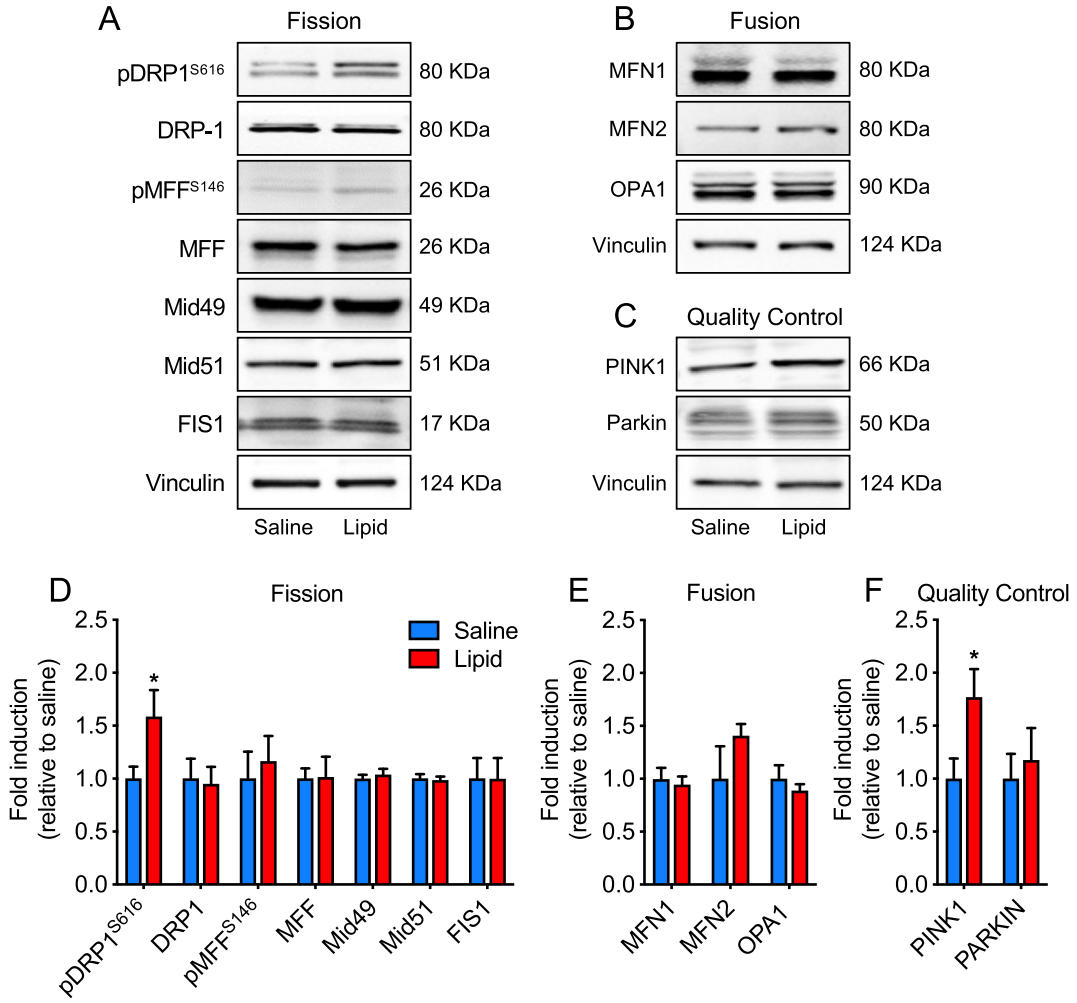

Fig. 3. Expression of proteins regulating mitochondrial fission, fusion, and quality control. **(A-C)** Representative immunoblots of phosphorylated and total DRP1 and MFF, Mid49, Mid51, FIS1, MFN1, MFN2, OPA1, PINK1, Parkin, and Vinculin (loading control). **(D-E)** Densitometric quantification of protein expression relative to saline treatment. Data are shown as the mean ± SEM. *$p < 0.05$. Comparisons of treatment were assessed by paired Students *t*-test.

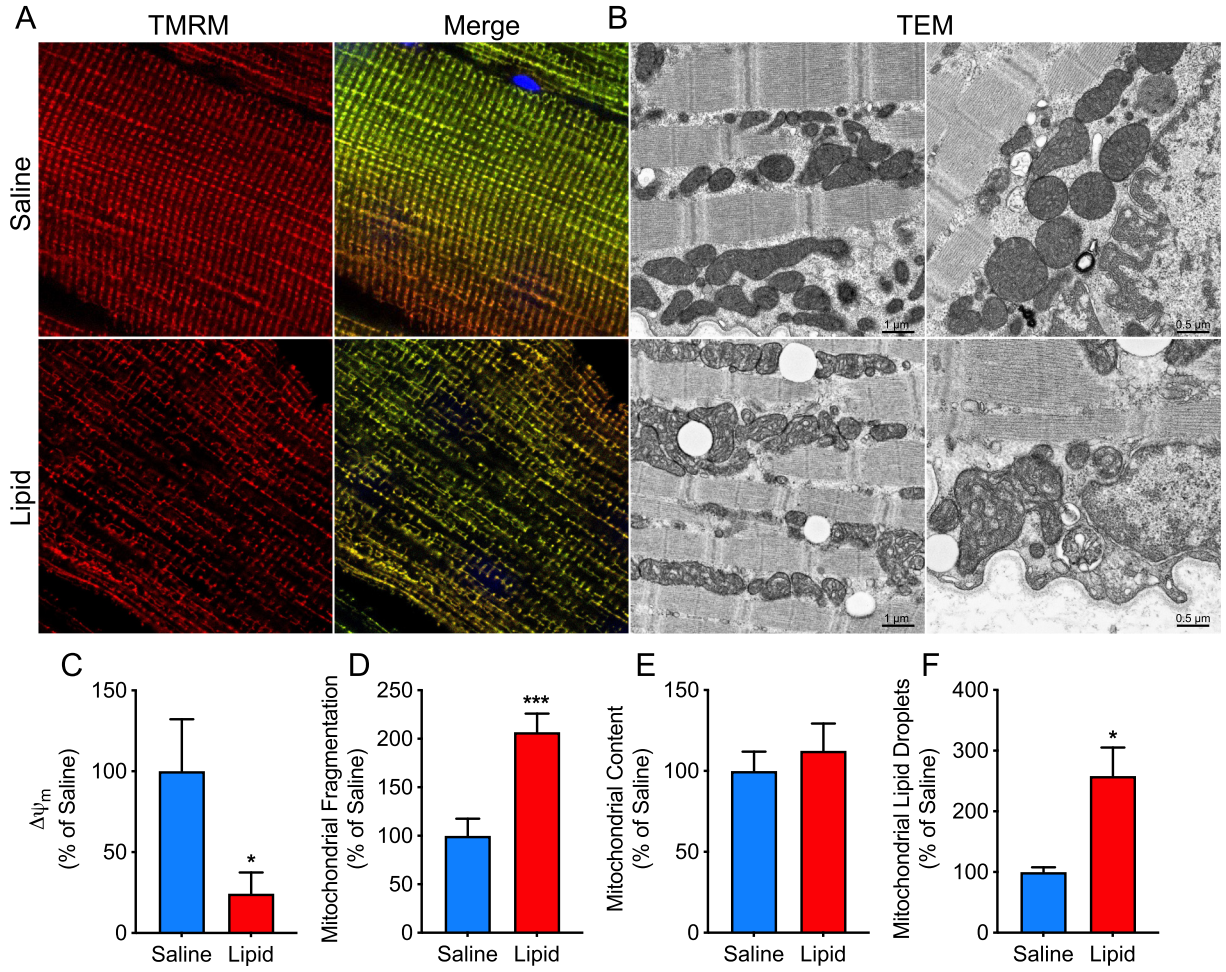

Fig. 4. Mitochondrial membrane potential and ultrastructure. **(A)** Representative confocal micrographs of resting mitochondrial membrane potential ($\Delta\psi_m$; 150× magnification). Micrographs are shown as TMRM alone (left) or the merge of TMRM, mitotracker deep red, and DAPI. **(B)** Transmission electron micrographs of mitochondrial ultrastructure and content (Scale bars (black) = 2 μm). Quantitation of **(C)** $\Delta\psi_m$, **(D)** mitochondrial fragmentation, **(E)** mitochondrial content, and **(F)** mitochondrial associated lipid droplets. Differences are represented relative to saline (%). Data are shown as the mean ± SEM. *p < 0.05. Comparisons of treatment were assessed by paired Students t-test. (For interpretation of the references to colour in this figure legend, the reader is referred to the web version of this article.)

triglycerides (64.2 ± 8.7 vs. 203.7 ± 39.5 mg/dL, P < 0.001) and very low-density lipoproteins (12.9 ± 1.9 vs. 31.2 ± 5.5 mg/dL, $P = 0.009$), and decreased high-density lipoproteins (53.7 ± 3.1 vs. 48.2 ± 3.2 mg/dL, P = 0.009) (Table 2). Furthermore, suppression of FFAs by insulin stimulation was significantly lower (79.8 ± 6.7 vs. 60.6 ± 3.7%, $P = 0.019$) following the lipid infusion (Fig. 7B). Resting energy expenditure and oxidation of carbohydrates and fat were unaltered by lipid infusion (Fig. 7C-E). However, metabolic flexibility, defined as the change in fat oxidation from basal to insulin stimulation, was lower (0.08 ± 0.01 vs. -0.03 ± 0.01 g/min, $P = 0.029$) following the overnight lipid infusion (Fig. 7F).

4. Discussion

DRP1-mediated skeletal muscle mitochondrial fission has previously been shown to contribute to insulin resistance in vitro and in murine models of obesity [21]. However, such models cannot account for 1) the biological concentrations of lipids that reach skeletal muscle as compared to other metabolic organs, and 2) how the metabolic milieu in humans can contribute to mitochondrial fission/fusion dynamics. Here, sedentary but otherwise healthy adults were prospectively randomized to receive either lipid or saline infusion to isolate the direct contribution of fatty acids to skeletal muscle mitochondrial dynamics. We observed that the lipid infusion increased DRP1-mediated mitochondrial fission and fragmentation which was observed in concert with transient reductions in hepatic and peripheral insulin sensitivity. Interestingly, the lipid infusion, despite increasing mitochondrial associated lipid droplet formation and contact sites, had no effect on the number or size of mitochondria themselves, indicating a more direct effect on membrane dynamics and morphology. Increased mitochondrial fragmentation has been observed in skeletal muscle and cultured myotubes from patients with obesity and type 2 diabetes compared to healthy participants and is partially restored by intensive weight loss [39–42]. Similarly, hyperactivation of DRP1 in the dorsal vagal complex in response to high fat feeding in rodents impairs glucose uptake and insulin signaling [43]. Though mitochondrial fusion was unaltered by lipid infusion, MFN2 gene and protein expression has been previously observed to be lower in humans and rodents with obesity [44,45]. MFN2 expression is restored following progressive weight loss [46] which is dependent on activation of the peroxisome proliferator-activated receptor gamma coactivator-1, a master regulator of mitochondrial biogenesis [46]. Furthermore, MFN2 deficiency in rodents results in hepatic and skeletal muscle insulin resistance [47]. It is therefore likely that obesity and type 2 diabetes related reductions in mitochondrial volume and biogenesis account for changes in mitochondrial fusion [6,22]. Additionally, we observed increased PINK1 expression and the presence of autophagic vesicles in response to lipid infusion, indicating that mitochondrial turnover is highly responsive to nutrient excess. These

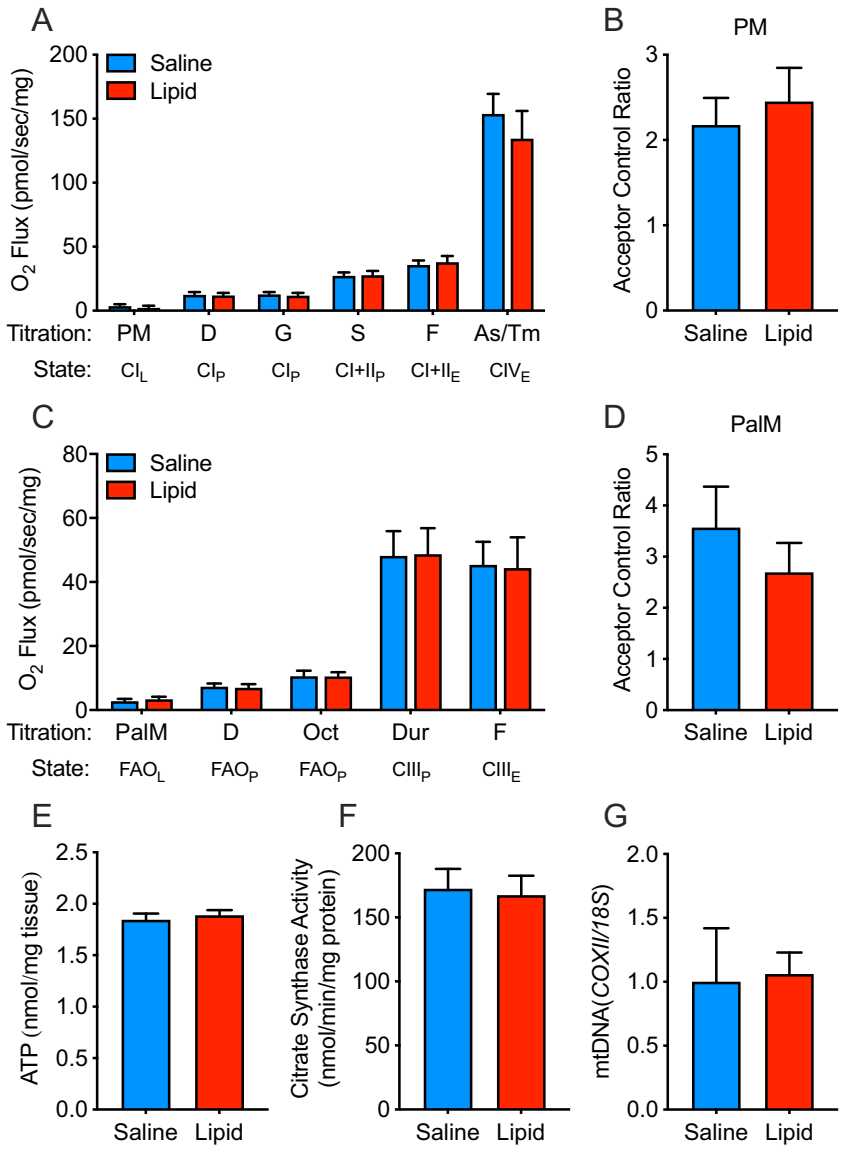

Fig. 5. Oxidative phosphorylation and electron transfer capacity. **(A-B)** Assessment of leak respiration (L), OXPHOS (P) and ET (E) capacity in permeabilized skeletal muscle fibers. **(C)** Ratio of maximal ADP-stimulated O_2 flux in the presence of pyruvate and malate to the leak rate in the absence in ADP. **(D)** Ratio of maximal ADP-stimulated O_2 flux in the presence of palmitoylcarnitine to the leak rate in the absence in ADP. **(E)** Tissue concentrations of ATP. **(F)** Enzymatic activity of citrate synthase. **(G)** mtDNA content (*COXII/18S*). PM: pyruvate and malate, D: adenosine diphosphate, G: glutamate, S: succinate, F: FCCP, As: ascorbate, Tm: tetramethyl-*p*-phenylenediamine, PalM: palmitoylcarnitine and malate, Oct: octanoylcarnitine, and Dur: duroquinol. Data are shown as the mean ± SEM. Comparisons of treatment x time were assessed by two-way repeated measures ANOVA with Tukey's multiple comparisons. Comparisons of treatment were assessed by paired Students t-test.

findings are supported by PINK1 loss of function models where glucose uptake is reduced by ~30%, and by negative associations between glycated end products and PINK1 expression in human skeletal muscle [48]. Under these circumstances, it is most likely that DRP1-mediated fission results in dampening of $\Delta\Psi_m$ and accumulation of PINK1 on depolarized mitochondrial membranes. Over time, increased fission events and accumulation of depolarized mitochondria would reduce the network volume, which has been widely reported in patients with obesity and type 2 diabetes [6,49,50].

Previous reports indicate that defects in electron transport chain activities, ATP production, and phosphocreatine recovery are present in humans with obesity and type 2 diabetes [5,51–54]. However, reductions in oxidative function can be accounted for by reductions in respiratory enzymes and mitochondrial DNA content, and markers of skeletal muscle mitochondrial content, in humans with obesity and type 2 diabetes [6]. Here, we show that both OXPHOS and ETC capacity, fatty acid oxidation, intracellular ATP, and markers of mitochondrial content are entirely intact following lipid infusion. It was unexpected that the lipid infusion lowered $\Delta\Psi m$ without altering bioenergetic efficiency or ATP production. Based upon these findings, we posit that the biological role of DRP1-mediated mitochondrial fission in response to a high lipid milieu is to limit mitochondrial substrate flow, and therefore ensure functional integrity of the remaining network. This is supported by observations under conditions of starvation or low nutrient supply where DRP1-mediated fission is largely inhibited, favoring elongated, tubular mitochondrial networks that can serve to increase bioenergetic efficiency and ATP supply [55]. Furthermore, evidence from cryo-EM studies have revealed that DRP1 interacts directly with phospholipids, such as cardiolipin, to coordinate DRP1 activation and oligomerization [56]. In contrast, intact membrane potential is required for OXPHOS control and coupling efficiency [57].

We, and others, have previously shown that short-term infusion of lipids is sufficient to reduce skeletal muscle and hepatic insulin sensitivity by modest induction of hyperglycemia and hyperinsulinemia in

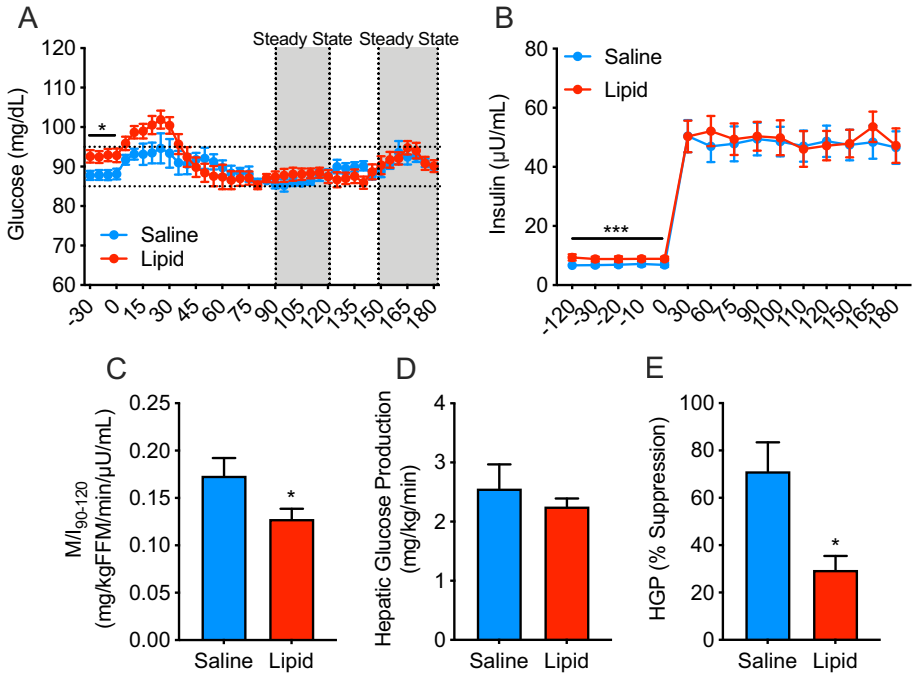

Fig. 6. Glucose homeostasis and insulin sensitivity. **(A)** Fasting glucose and clamp-derived euglycemia, **(B)** fasting insulin and clamp-derived hyperinsulinemia. **(C)** peripheral insulin sensitivity, **(D)** basal rate of HGP, and **(E)** suppression of HGP by insulin. Data are shown as the mean ± SEM. *p < 0.05, **p < 0.01, ***p < 0.01. Comparisons of treatment x time were assessed by two-way repeated measures ANOVA with Tukey's multiple comparisons. Comparisons of treatment were assessed by paired Students t-test.

healthy subjects [58–62]. The role of lipids in insulin resistance and type 2 diabetes is further evidenced by the marked elevation in circulating FFAs and insulin in persons with obesity and type 2 diabetes [63]. However, the mechanisms by which excess FFAs are linked to impaired glucose utilization remain unclear. One view posits that nutrient overload can cause a build-up of intermediary metabolites, products of incomplete oxidation such as acyl-CoAs and acylcarnitines, in the mitochondria [64] and that these moieties inhibit insulin signaling directly [65], or indirectly by forming lipid species [66] that activate inflammatory cascades [67,68], oxidative stress signaling [69] and stress kinases

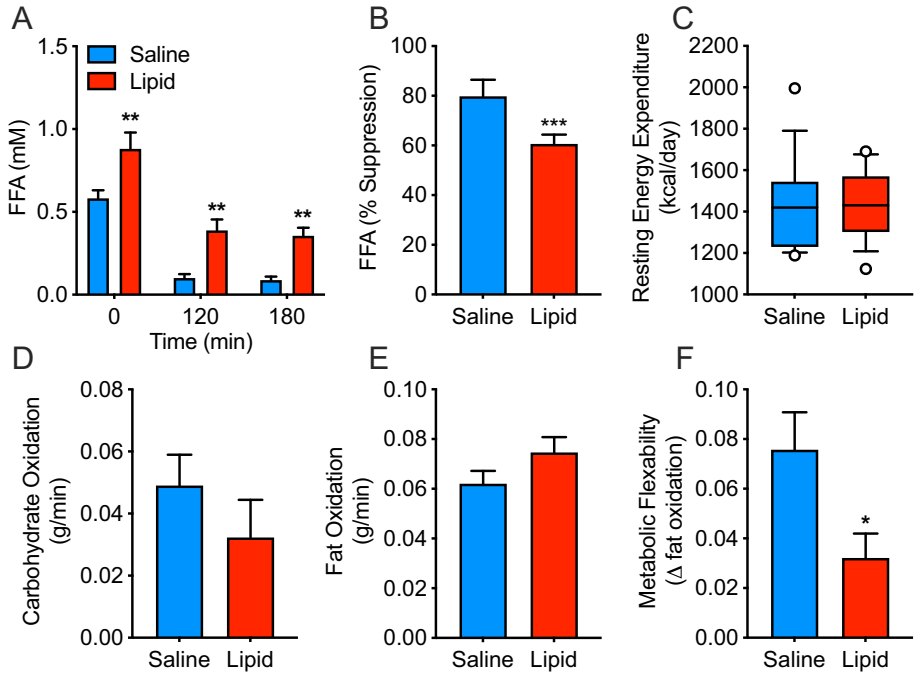

Fig. 7. Whole-body substrate metabolism. **(A)** Fasting and insulin stimulated FFAs and **(B)** suppression of FFA's in response to insulin stimulation. Basal **(C)** carbohydrate, **(D)** protein, **(E)** and fat oxidation rates. **(F)** Change in the rate of fat oxidation from basal to insulin stimulation. Data are shown as the mean ± SEM with exception to panel C which is displayed as a box (mean) and whiskers (10–90% CI). *p < 0.05, **p < 0.01, ***p < 0.01. Comparisons of treatment x time were assessed by two-way repeated measures ANOVA with Tukey's multiple comparisons. Comparisons of treatment were assessed by paired Students t-test.

such as the PKCs [70,71]. However, skeletal muscle deletion of carnitine palmitoyltransferase-1, the rate-limiting enzyme for acyl-CoA transport into the mitochondria for oxidation, does not impair glycemic control or insulin sensitivity [72]. Based upon our findings, we posit that DRP1-mediated mitochondrial fission may facilitate the release of intermediary metabolites [73] into the cytosol which can directly suppress nutrient uptake by the cell [74]. Since depolarized mitochondria do not completely oxidize substrate [57], even transiently depolarized mitochondria would promote substrate catabolism without affecting ATP content, and the production of additional intermediary metabolites would further inhibit nutrient uptake. However, further investigation is required to demonstrate this mechanism in humans.

5. Conclusion

Our data suggest that mitochondrial fission and quality control networks are activated in response to lipid infusion which occurs independent of changes in mitochondrial content or capacity and contributes to the onset of insulin resistance in healthy humans. Treatments that limit lipid-induced activation of mitochondrial fission and/or quality control processes may have therapeutic value in the treatment insulin resistance as an underlying pathophysiology of numerous metabolic diseases such as obesity and type 2 diabetes.

5.1. Limitations of study

Our study employed an intravenous infusion model to provide a constant, low dose administration of lipids to participants over a 12-hr period of time. This approach controlled for the confounding post-prandial effects of the enteroinsular axis on skeletal muscle lipid supply and insulin sensitivity. However, in a free-living environment, changes in lipid supply occur intermittently throughout the feeding window concordant with post-prandial fluctuation in FFA availability. As such, we cannot conclude that activation of DRP1 would occur after a single or repeated high fat meals.

Funding

This research was supported by National Institutes of Health grants R01 DK108089 (JPK), U54 GM104940 (JPK), T32 AT004094 (JTM), and T32 DK064584 (MLE). The authors declare no competing interests. John P. Kirwan is the guarantor of this work and, as such, had full access to all data in the study and takes responsibility for the integrity and accuracy of the data analysis.

CRediT authorship contribution statement

Christopher L. Axelrod: Conceptualization, Methodology, Formal analysis, Investigation, Data curation, Writing – original draft, Visualization, Project administration. **Ciaran E. Fealy:** Conceptualization, Methodology, Investigation, Writing – review & editing. **Melissa L. Erickson:** Investigation, Data curation, Writing – review & editing. **Gangarao Davuluri:** Investigation, Writing – review & editing. **Hisashi Fujioka:** Formal analysis, Investigation, Writing – review & editing. **Wagner S. Dantas:** Formal analysis, Investigation, Writing – review & editing. **Emily Huang:** Investigation, Writing – review & editing. **Kathryn Pergola:** Validation, Investigation, Data curation, Writing – review & editing, Visualization. **Jacob T. Mey:** Investigation, Writing – review & editing. **William T. King:** Investigation, Writing – review & editing. **Anny Mulya:** Investigation, Writing – review & editing. **Daniel Hsia:** Investigation, Supervision, Writing – review & editing. **Bartolome Burguera:** Investigation, Supervision, Writing – review & editing. **Bernard Tandler:** Formal analysis, Investigation, Writing – review & editing. **Charles L. Hoppel:** Conceptualization, Methodology, Formal analysis, Investigation, Resources, Data curation, Writing – review & editing, Supervision. **John P. Kirwan:** Conceptualization, Methodology, Investigation, Resources, Writing – review & editing, Supervision, Project administration, Funding acquisition.

Declaration of competing interest

The authors declare that there are no conflicts of interest.

Acknowledgements

We thank the Cleveland Clinic, Clinical Research Unit and the Pennington Biomedical Research Center Inpatient Unit for providing patient care and research support. We thank the study volunteers for their considerable time and effort in the trial.

References

[1] Samuel VT, Petersen KF, Shulman GI. Lipid-induced insulin resistance: unravelling the mechanism. Lancet. 2010;375:2267–77.
[2] Yu C, Chen Y, Cline GW, Zhang D, Zong H, Wang Y, et al. Mechanism by which fatty acids inhibit insulin activation of insulin receptor substrate-1 (IRS-1)-associated phosphatidylinositol 3-kinase activity in muscle. J Biol Chem. 2002;277:50230–6.
[3] Haus JM, Kashyap SR, Kasumov T, Zhang R, Kelly KR, Defronzo RA, et al. Plasma ceramides are elevated in obese subjects with type 2 diabetes and correlate with the severity of insulin resistance. Diabetes. 2009;58:337–43.
[4] Szendroedi J, Phielix E, Roden M. The role of mitochondria in insulin resistance and type 2 diabetes mellitus. Nat Rev Endocrinol. 2011;8:92–103.
[5] Kelley DE, He J, Menshikova EV, Ritov VB. Dysfunction of mitochondria in human skeletal muscle in type 2 diabetes. Diabetes. 2002;51:2944–50.
[6] Boushel R, Gnaiger E, Schjerling P, Skovbro M, Kraunsoe R, Dela F. Patients with type 2 diabetes have normal mitochondrial function in skeletal muscle. Diabetologia. 2007;50:790–6.
[7] Turner N, Bruce CR, Beale SM, Hoehn KL, So T, Rolph MS, et al. Excess lipid availability increases mitochondrial fatty acid oxidative capacity in muscle: evidence against a role for reduced fatty acid oxidation in lipid-induced insulin resistance in rodents. Diabetes. 2007;56:2085–92.
[8] Fealy CE, Mulya A, Axelrod CL, Kirwan JP. Mitochondrial dynamics in skeletal muscle insulin resistance and type 2 diabetes. Transl Res. 2018;202:69–82.
[9] Gao AW, Canto C, Houtkooper RH. Mitochondrial response to nutrient availability and its role in metabolic disease. EMBO Mol Med. 2014;6:580–9.
[10] Detmer SA, Chan DC. Functions and dysfunctions of mitochondrial dynamics. Nat Rev Mol Cell Biol. 2007;8:870–9.
[11] Kwong JQ, Molkentin JD. Physiological and pathological roles of the mitochondrial permeability transition pore in the heart. Cell Metab. 2015;21:206–14.
[12] Westermann B. Mitochondrial fusion and fission in cell life and death. Nat Rev Mol Cell Biol. 2010;11:872–84.
[13] Loson OC, Song Z, Chen H, Chan DC. Fis1, Mff, MiD49, and MiD51 mediate Drp1 recruitment in mitochondrial fission. Mol Biol Cell. 2013;24:659–67.
[14] Bleazard W, McCaffery JM, King EJ, Bale S, Mozdy A, Tieu Q, et al. The dynamin-related GTPase Dnm1 regulates mitochondrial fission in yeast. Nat Cell Biol. 1999;1:298–304.
[15] Kashatus JA, Nascimento A, Myers LJ, Sher A, Byrne FL, Hoehn KL, et al. Erk2 phosphorylation of Drp1 promotes mitochondrial fission and MAPK-driven tumor growth. Mol Cell. 2015;57:537–51.
[16] Mears JA, Lackner LL, Fang S, Ingerman E, Nunnari J, Hinshaw JE. Conformational changes in Dnm1 support a contractile mechanism for mitochondrial fission. Nat Struct Mol Biol. 2011;18:20–6.
[17] Frank S, Gaume B, Bergmann-Leitner ES, Leitner WW, Robert EG, Catez F, et al. The role of dynamin-related protein 1, a mediator of mitochondrial fission, in apoptosis. Dev Cell. 2001;1:515–25.
[18] Narendra DP, Jin SM, Tanaka A, Suen DF, Gautier CA, Shen J, et al. PINK1 is selectively stabilized on impaired mitochondria to activate Parkin. PLoS Biol. 2010;8:e1000298.
[19] Griffin EE, Detmer SA, Chan DC. Molecular mechanism of mitochondrial membrane fusion. Biochim Biophys Acta. 1763;2006:482–9.
[20] Ge Y, Shi X, Boopathy S, McDonald J, Smith AW, Chao LH. Two forms of Opa1 cooperate to complete fusion of the mitochondrial inner-membrane. Elife. 2020;9.
[21] Jheng HF, Tsai PJ, Guo SM, Kuo LH, Chang CS, Su IJ, et al. Mitochondrial fission contributes to mitochondrial dysfunction and insulin resistance in skeletal muscle. Mol Cell Biol. 2012;32:309–19.
[22] Axelrod CL, Fealy CE, Mulya A, Kirwan JP. Exercise training remodels human skeletal muscle mitochondrial fission and fusion machinery towards a pro-elongation phenotype. Acta Physiol (Oxf) 2019;225:e13216.
[23] DeFronzo RA, Tobin JD, Andres R. Glucose clamp technique: a method for quantifying insulin secretion and resistance. Am J Physiol. 1979;237:E214–23.
[24] Fealy CE, Mulya A, Lai N, Kirwan JP. Exercise training decreases activation of the mitochondrial fission protein dynamin-related protein-1 in insulin-resistant human skeletal muscle. J Appl Physiol (1985). 2014;117:239–45.
[25] Steele R, Wall JS, De Bodo RC, Altszuler N. Measurement of size and turnover rate of body glucose pool by the isotope dilution method. Am J Physiol. 1956;187:15–24.
[26] Frayn KN. Calculation of substrate oxidation rates in vivo from gaseous exchange. J Appl Physiol Respir Environ Exerc Physiol. 1983;55:628–34.
[27] Evans WJ, Phinney SD, Young VR. Suction applied to a muscle biopsy maximizes sample size. Med Sci Sports Exerc. 1982;14:101–2.
[28] Schneider CA, Rasband WS, Eliceiri KW. NIH image to ImageJ: 25 years of image analysis. Nat Methods. 2012;9:671–5.

[29] Ye F, Hoppel CL. Measuring oxidative phosphorylation in human skin fibroblasts. Anal Biochem. 2013;437:52–8.
[30] Chavez AO, Kamath S, Jani R, Sharma LK, Monroy A, Abdul-Ghani MA, et al. Effect of short-term free fatty acids elevation on mitochondrial function in skeletal muscle of healthy individuals. J Clin Endocrinol Metab. 2010;95:422–9.
[31] Halling JF, Ringholm S, Olesen J, Prats C, Pilegaard H. Exercise training protects against aging-induced mitochondrial fragmentation in mouse skeletal muscle in a PGC-1alpha dependent manner. Exp Gerontol. 2017;96:1–6.
[32] Fujioka H, Tandler B, Hoppel CL. Mitochondrial division in rat cardiomyocytes: an electron microscope study. Anat Rec (Hoboken). 2012;295:1455–61.
[33] Kalt MR, Tandler B. A study of fixation of early amphibian embryos for electron microscopy. J Ultrastruct Res. 1971;36:633–45.
[34] Tandler B. Improved uranyl acetate staining for electron microscopy. J Electron Microsc Tech. 1990;16:81–2.
[35] Hanaichi T, Sato T, Iwamoto T, Malavasi-Yamashiro J, Hoshino M, Mizuno N. A stable lead by modification of Sato's method. J Electron Microsc (Tokyo). 1986;35:304–6.
[36] Axelrod CL, King WT, Davuluri G, Noland RC, Hall J, Hull M, et al. BAM15-mediated mitochondrial uncoupling protects against obesity and improves glycemic control. EMBO Mol Med. 2020;12:e12088.
[37] Yoon JC, Ng A, Kim BH, Bianco A, Xavier RJ, Elledge SJ. Wnt signaling regulates mitochondrial physiology and insulin sensitivity. Genes Dev. 2010;24:1507–18.
[38] Solomon TP, Haus JM, Kelly KR, Cook MD, Filion J, Rocco M, et al. A low-glycemic index diet combined with exercise reduces insulin resistance, postprandial hyperinsulinemia, and glucose-dependent insulinotropic polypeptide responses in obese, prediabetic humans. Am J Clin Nutr. 2010;92:1359–68.
[39] Boyle KE, Zheng D, Anderson EJ, Neufer PD, Houmard JA. Mitochondrial lipid oxidation is impaired in cultured myotubes from obese humans. Int J Obes (Lond) 2012;36:1025–31.
[40] Gundersen AE, Kugler BA, McDonald PM, Veraksa A, Houmard JA, Zou K. Altered mitochondrial network morphology and regulatory proteins in mitochondrial quality control in myotubes from severely obese humans with or without type 2 diabetes. Appl Physiol Nutr Metab. 2020;45:283–93.
[41] Kristensen CM, Jessen H, Ringholm S, Pilegaard H. Muscle PGC-1alpha in exercise and fasting-induced regulation of hepatic UPR in mice. Acta Physiol (Oxf) 2018;224:e13158.
[42] Kugler BA, Gundersen AE, Li J, Deng W, Eugene N, Gona PN, et al. Roux-en-Y gastric bypass surgery restores insulin-mediated glucose partitioning and mitochondrial dynamics in primary myotubes from severely obese humans. Int J Obes (Lond) 2020;44:684–96.
[43] Filippi BM, Abraham MA, Silva PN, Rasti M, LaPierre MP, Bauer PV, et al. Dynamin-related protein 1-dependent mitochondrial fission changes in the dorsal vagal complex regulate insulin action. Cell Rep. 2017;18:2301–9.
[44] Bach D, Pich S, Soriano FX, Vega N, Baumgartner B, Oriola J, et al. Mitofusin-2 determines mitochondrial network architecture and mitochondrial metabolism. A novel regulatory mechanism altered in obesity. J Biol Chem. 2003;278:17190–7.
[45] Bach D, Naon D, Pich S, Soriano FX, Vega N, Rieusset J, et al. Expression of Mfn2, the Charcot-Marie-tooth neuropathy type 2A gene, in human skeletal muscle: effects of type 2 diabetes, obesity, weight loss, and the regulatory role of tumor necrosis factor alpha and interleukin-6. Diabetes. 2005;54:2685–93.
[46] Gastaldi G, Russell A, Golay A, Giacobino JP, Habicht F, Barthassat V, et al. Upregulation of peroxisome proliferator-activated receptor gamma coactivator gene (PGC1A) during weight loss is related to insulin sensitivity but not to energy expenditure. Diabetologia. 2007;50:2348–55.
[47] Sebastian D, Hernandez-Alvarez MI, Segales J, Sorianello E, Munoz JP, Sala D, et al. Mitofusin 2 (Mfn2) links mitochondrial and endoplasmic reticulum function with insulin signaling and is essential for normal glucose homeostasis. Proc Natl Acad Sci U S A. 2012;109:5523–8.
[48] Scheele C, Nielsen AR, Walden TB, Sewell DA, Fischer CP, Brogan RJ, et al. Altered regulation of the PINK1 locus: a link between type 2 diabetes and neurodegeneration? FASEB J. 2007;21:3653–65.
[49] Ritov VB, Menshikova EV, He J, Ferrell RE, Goodpaster BH, Kelley DE. Deficiency of subsarcolemmal mitochondria in obesity and type 2 diabetes. Diabetes. 2005;54:8–14.
[50] Holloway GP, Thrush AB, Heigenhauser GJ, Tandon NN, Dyck DJ, Bonen A, et al. Skeletal muscle mitochondrial FAT/CD36 content and palmitate oxidation are not decreased in obese women. Am J Physiol Endocrinol Metab. 2007;292:E1782–9.
[51] Schrauwen-Hinderling VB, Kooi ME, Hesselink MK, Jeneson JA, Backes WH, van Echteld CJ, et al. Impaired in vivo mitochondrial function but similar intramyocellular lipid content in patients with type 2 diabetes mellitus and BMI-matched control subjects. Diabetologia. 2007;50:113–20.
[52] Simoneau JA, Veerkamp JH, Turcotte LP, Kelley DE. Markers of capacity to utilize fatty acids in human skeletal muscle: relation to insulin resistance and obesity and effects of weight loss. FASEB J. 1999;13:2051–60.
[53] Anderson EJ, Lustig ME, Boyle KE, Woodlief TL, Kane DA, Lin CT, et al. Mitochondrial H2O2 emission and cellular redox state link excess fat intake to insulin resistance in both rodents and humans. J Clin Invest. 2009;119:573–81.
[54] Asmann YW, Stump CS, Short KR, Coenen-Schimke JM, Guo Z, Bigelow ML, et al. Skeletal muscle mitochondrial functions, mitochondrial DNA copy numbers, and gene transcript profiles in type 2 diabetic and nondiabetic subjects at equal levels of low or high insulin and euglycemia. Diabetes. 2006;55:3309–19.
[55] Rambold AS, Kostelecky B, Elia N, Lippincott-Schwartz J. Tubular network formation protects mitochondria from autophagosomal degradation during nutrient starvation. Proc Natl Acad Sci U S A. 2011;108:10190–5.
[56] Francy CA, Clinton RW, Frohlich C, Murphy C, Mears JA. Cryo-EM studies of Drp1 reveal cardiolipin interactions that activate the helical oligomer. Sci Rep. 2017;7:10744.
[57] Zorova LD, Popkov VA, Plotnikov EY, Silachev DN, Pevzner IB, Jankauskas SS, et al. Mitochondrial membrane potential. Anal Biochem. 2018;552:50–9.
[58] Roden M, Price TB, Perseghin G, Petersen KF, Rothman DL, Cline GW, et al. Mechanism of free fatty acid-induced insulin resistance in humans. J Clin Invest. 1996;97:2859–65.
[59] Kashyap SR, Belfort R, Berria R, Suraamornkul S, Pratipranawatr T, Finlayson J, et al. Discordant effects of a chronic physiological increase in plasma FFA on insulin signaling in healthy subjects with or without a family history of type 2 diabetes. Am J Physiol Endocrinol Metab. 2004;287:E537–46.
[60] Shah P, Vella A, Basu A, Basu R, Adkins A, Schwenk WF, et al. Elevated free fatty acids impair glucose metabolism in women: decreased stimulation of muscle glucose uptake and suppression of splanchnic glucose production during combined hyperinsulinemia and hyperglycemia. Diabetes. 2003;52:38–42.
[61] Solomon TP, Haus JM, Marchetti CM, Stanley WC, Kirwan JP. Effects of exercise training and diet on lipid kinetics during free fatty acid-induced insulin resistance in older obese humans with impaired glucose tolerance. Am J Physiol Endocrinol Metab. 2009;297:E552–9.
[62] Liu Z, Liu J, Jahn LA, Fowler DE, Barrett EJ. Infusing lipid raises plasma free fatty acids and induces insulin resistance in muscle microvasculature. J Clin Endocrinol Metab. 2009;94:3543–9.
[63] Reaven GM, Hollenbeck C, Jeng CY, Wu MS, Chen YD. Measurement of plasma glucose, free fatty acid, lactate, and insulin for 24 h in patients with NIDDM. Diabetes. 1988;37:1020–4.
[64] Koves TR, Ussher JR, Noland RC, Slentz D, Mosedale M, Ilkayeva O, et al. Mitochondrial overload and incomplete fatty acid oxidation contribute to skeletal muscle insulin resistance. Cell Metab. 2008;7:45–56.
[65] Schooneman MG, Vaz FM, Houten SM, Soeters MR. Acylcarnitines: reflecting or inflicting insulin resistance? Diabetes. 2013;62:1–8.
[66] Keung W, Ussher JR, Jaswal JS, Raubenheimer M, Lam VH, Wagg CS, et al. Inhibition of carnitine palmitoyltransferase-1 activity alleviates insulin resistance in diet-induced obese mice. Diabetes. 2013;62:711–20.
[67] Liang H, Tantiwong P, Sriwijitkamol A, Shanmugasundaram K, Mohan S, Espinoza S, et al. Effect of a sustained reduction in plasma free fatty acid concentration on insulin signalling and inflammation in skeletal muscle from human subjects. J Physiol. 2013;591:2897–909.
[68] Mehta NN, McGillicuddy FC, Anderson PD, Hinkle CC, Shah R, Pruscino L, et al. Experimental endotoxemia induces adipose inflammation and insulin resistance in humans. Diabetes. 2010;59:172–81.
[69] Muscogiuri G, Salmon AB, Aguayo-Mazzucato C, Li M, Balas B, Guardado-Mendoza R, et al. Genetic disruption of SOD1 gene causes glucose intolerance and impairs beta-cell function. Diabetes. 2013;62:4201–7.
[70] Considine RV, Caro JF. Protein kinase C: mediator or inhibitor of insulin action? J Cell Biochem. 1993;52:8–13.
[71] Nowotny B, Zahiragic L, Krog D, Nowotny PJ, Herder C, Carstensen M, et al. Mechanisms underlying the onset of oral lipid-induced skeletal muscle insulin resistance in humans. Diabetes. 2013;62:2240–8.
[72] Wicks SE, Vandanmagsar B, Haynie KR, Fuller SE, Warfel JD, Stephens JM, et al. Impaired mitochondrial fat oxidation induces adaptive remodeling of muscle metabolism. Proc Natl Acad Sci U S A. 2015;112:E3300–9.
[73] Itani SI, Ruderman NB, Schmieder F, Boden G. Lipid-induced insulin resistance in human muscle is associated with changes in diacylglycerol, protein kinase C, and IkappaB-alpha. Diabetes. 2002;51:2005–11.
[74] Boden G, Chen X, Ruiz J, White JV, Rossetti L. Mechanisms of fatty acid-induced inhibition of glucose uptake. J Clin Invest. 1994;93:2438–46.